Rapid Communications

Revising the $4f$ symmetry in $CeCu_2Ge_2$: Soft x-ray absorption and hard x-ray photoemission spectroscopy

H. Aratani,[1,2] Y. Nakatani,[1,2] H. Fujiwara,[1,2,*] M. Kawada,[1,2] Y. Kanai,[1,2] K. Yamagami,[1,2] S. Fujioka,[1,2] S. Hamamoto,[1,2] K. Kuga,[2] T. Kiss,[1,2] A. Yamasaki,[2,3] A. Higashiya,[2,4] T. Kadono,[2,5] S. Imada,[2,5] A. Tanaka,[6] K. Tamasaku,[2] M. Yabashi,[2] T. Ishikawa,[2] A. Yasui,[7] Y. Saitoh,[8] Y. Narumi,[9,†] K. Kindo,[9] T. Ebihara,[10] and A. Sekiyama[1,2]

[1]*Division of Materials Physics, Graduate School of Engineering Science, Osaka University, Toyonaka, Osaka 560-8531, Japan*

[2]*RIKEN SPring-8 Center, Sayo, Hyogo 679-5148, Japan*

[3]*Faculty of Science and Engineering, Konan University, Kobe 658-8501, Japan*

[4]*Faculty of Science and Engineering, Setsunan University, Neyagawa, Osaka 572-8508, Japan*

[5]*Department of Physical Sciences, Ritsumeikan University, Kusatsu, Shiga 525-8577, Japan*

[6]*Department of Quantum Matter, ADSM, Hiroshima University, Higashi-hiroshima, Hiroshima 739-8530, Japan*

[7]*Japan Synchrotron Radiation Research Institute (JASRI), Sayo, Hyogo 679-5198, Japan*

[8]*Materials Sciences Research Center, Japan Atomic Energy Agency (JAEA), Sayo, Hyogo 679-5148, Japan*

[9]*The Institute for Solid State Physics, The University of Tokyo, Kashiwa, Chiba 277-8581, Japan*

[10]*Department of Physics, Shizuoka University, Shizuoka 422-8529, Japan*

(Received 6 February 2018; revised manuscript received 6 September 2018; published 28 September 2018)

We present a detailed study on the $4f$ ground-state symmetry of the pressure-induced superconductor $CeCu_2Ge_2$ probed by soft x-ray absorption and hard x-ray photoemission spectroscopy. The revised Ce $4f$ ground states are determined as $|\Gamma_7\rangle = \sqrt{0.45}\,|J_z = \pm\frac{5}{2}\rangle - \sqrt{0.55}\,|\mp\frac{3}{2}\rangle$ with Σ-type in-plane rotational symmetry. This gives an in-plane magnetic moment consistent with the antiferromagnetic moment as reported in neutron measurements. Since the in-plane symmetry is the same as that for the superconductor $CeCu_2Si_2$, we propose that the charge distribution along the c axis plays an essential role in driving the system into a superconducting phase.

DOI: 10.1103/PhysRevB.98.121113

The discovery of the first heavy fermion superconductor $CeCu_2Si_2$ has attracted considerable attention to quantum critical phenomena in strongly correlated electron systems [1–4] such as high-T_c superconductivity and topological phases with strong spin-orbit interactions [5,6]. The superconductivity in $CeCu_2Si_2$ is suppressed by the isostructural substitution of Ge for Si [7,8]. The end-member compound tetragonal $CeCu_2Ge_2$ shows an antiferromagnetic long-range order below a Néel temperature (T_N) of ∼4.2 K at ambient pressure [9]. The Sommerfeld coefficient γ is as high as 100 mJ/(mol K^2), suggesting that the energy scale of the on-site Kondo fluctuation is the same order of magnitude as that of the Ruderman-Kittel-Kasuya-Yosida (RKKY) interaction [9]. An external pressure above 7.6 GPa induces superconductivity below 0.6 K due largely to an increase of the hybridization between the localized $4f$ and conduction electrons. Moreover, a different type of superconducting phase emerges at around 12 GPa, where an abrupt change into the critical $4f$ valence fluctuation in the presence of a strong on-site Coulomb repulsion has been proposed to understand its origin [10–12].

The low-temperature properties of these compounds are mostly determined by the $4f$ ground-state symmetry for Ce^{3+} ions in the tetragonal crystalline electric field (CEF). The $4f$ states with a total angular momentum $J = 5/2$ split into three Kramers doublets equated to $|\Gamma_6\rangle = |J_z = \pm\frac{1}{2}\rangle$, $|\Gamma_7^1\rangle = \alpha\,|\pm\frac{5}{2}\rangle - \sqrt{1-\alpha^2}\,|\mp\frac{3}{2}\rangle$, and $|\Gamma_7^2\rangle = \sqrt{1-\alpha^2}\,|\pm\frac{5}{2}\rangle + \alpha\,|\mp\frac{3}{2}\rangle$, where α^2 denotes the mixing factor reflecting the out-of-plane (parallel to the crystal c axis) anisotropy in the spatial distribution of the $4f$ states. The α^2 value is also connected to the anisotropy in magnetic moments per Ce ion as shown in Fig. 1 [13,14]. The out-of-plane anisotropy can be determined by linearly polarized soft x-ray absorption spectroscopy (XAS) [15–17], and the phase diagram of tetragonal $CeIr_{1-x}Rh_xIn_5$ has shown to be scaled by α^2 [17]. Therefore, it has been recognized that proving ground-state symmetry is of great importance to elucidate the origin of quantum critical phenomena. In addition, the sign of α gives the in-plane (perpendicular to the c axis) rotational symmetry labeled as Σ-type (Π-type) Γ_7, whose charge distribution has valleys (crests) in the [100] direction as shown in Fig. 1(b). The in-plane symmetry for both $CeCu_2Si_2$ and $CeCu_2Ge_2$ has been determined as Σ-type Γ_7 using nonresonant inelastic x-ray scattering (NIXS) [18,19].

However, the CEF ground-state symmetry of $CeCu_2Ge_2$ is still puzzling. It has been reported that the $4f$ symmetry is described as $|\Gamma_7\rangle = 0.9\,|\pm\frac{5}{2}\rangle \pm 0.435\,|\mp\frac{3}{2}\rangle$ [20]. The corresponding α^2 value of 0.81 yields an expected magnetic moment of $\sim 1.5\mu_B$/Ce along the c axis as obtained from

*fujiwara@mp.es.osaka-u.ac.jp

†Present address: Center for Advanced High Magnetic Field Science, Graduate School of Science, Osaka University, Toyonaka, Osaka 560-0043, Japan.

 ©2018 American Physical Society

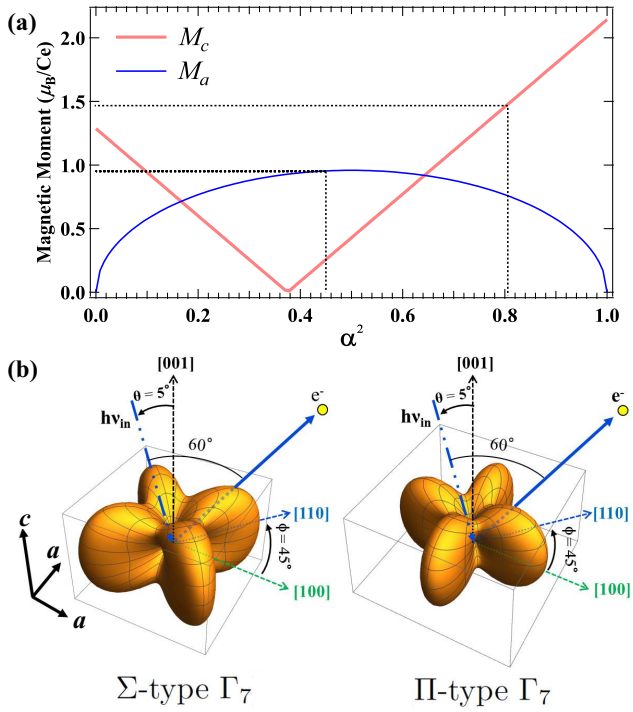

FIG. 1. (a) Expectation values of magnetic moments along the a and c axes per a Ce^{3+} ion denoted as M_a and M_c for the $|\Gamma_7\rangle = \alpha\,|\pm\frac{5}{2}\rangle \pm \sqrt{1-\alpha^2}\,|\mp\frac{3}{2}\rangle$ ground states plotted as a function of α^2. Dashed lines are guides for the eye for $\alpha^2 = 0.45$ and 0.81. (b) Angular distribution of charge density plot of the Γ_7 states with the possible rotational symmetry of Σ type (left) and Π type (right). In the HAXPES measurements, the angle between the incoming x ray (projection from an outgoing photoelectron to the ab plane) and the [001] direction ([100] direction) is defined as θ (ϕ).

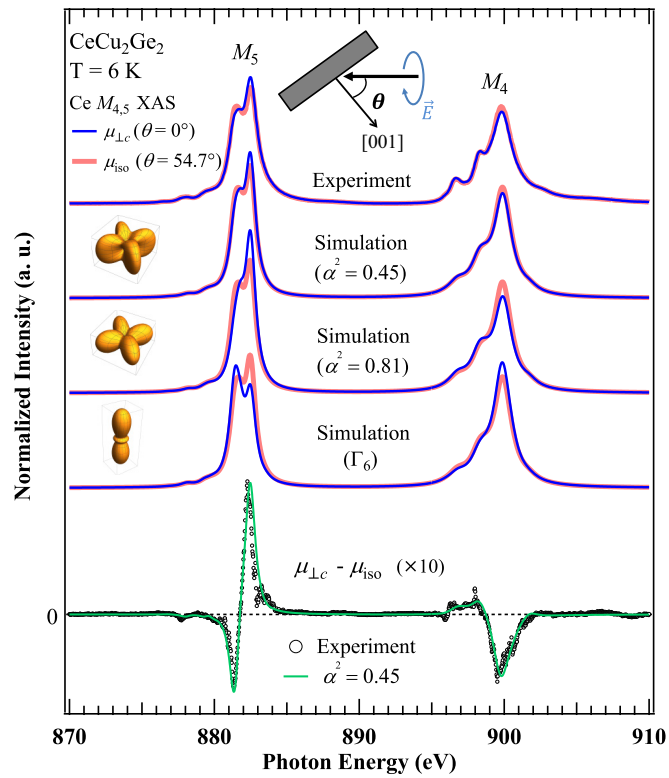

FIG. 2. Circularly polarized XAS spectra of $CeCu_2Ge_2$ at the Ce $M_{4,5}$ absorption edges (top) obtained for x-ray incidence angles of $\theta = 0°$ ($\mu_{\perp c}$) and 54.7° (μ_{iso}) with respect to the c axis parallel to the surface normal. The spectral simulations assuming the ground state of Γ_7 ($\alpha^2 = 0.45$), Γ_7 ($\alpha^2 = 0.81$), and Γ_6 symmetry together with the initial-state $4f$ charge distributions. The $\mu_{\perp c} - \mu_{iso}$ spectrum is compared with the best-fit simulation assuming Γ_7 ground states with $\alpha^2 = 0.45$ (bottom). The error bar of the experimental $\mu_{\perp c} - \mu_{iso}$ spectrum is within the size of the markers.

Fig. 1, which is much larger than a magnetic ordered moment of $1.04\mu_B$/Ce below T_N observed in neutron measurements [21–23]. It is also in sharp contrast to the Ce moments pointing in the ab plane [22,23]. Therefore, it is essential to determine the $4f$ ground-state symmetry of $CeCu_2Ge_2$ by utilizing advanced spectroscopy.

In this Rapid Communication, we report a revising ground-state symmetry of $CeCu_2Ge_2$ studied by the polarized XAS and hard x-ray photoemission spectroscopy (HAXPES). The mixing parameter α^2, obtained by XAS, successfully explains the magnetic susceptibility. By analyzing the Ce $3d$ core-level HAXPES spectra using the same α^2 value [24–26], in-plane symmetry of the $4f$ states is determined as Σ-type Γ_7, which is consistent with the results obtained from NIXS measurements [19].

High-quality $CeCu_2Ge_2$ single crystals were grown by the Cu-Ge flux method [27]. Magnetic susceptibility was measured by means of a superconducting quantum interface device (SQUID) magnetometer (Quantum Design, MPMS3). XAS measurements were performed at the twin-helical undulator beamline BL23SU of SPring-8 [28]. The XAS spectra were obtained in total-electron-yield mode with an energy resolution of 80 meV, and the base pressure was about 1.1×10^{-8} Pa. The HAXPES measurements were performed at BL19LXU of SPring-8 [29], where a MBS A1-HE hemispherical electron analyzer and transmission-type phase retarders were installed [30]. The degree of linear polarization (P_L) of the polarization-switched x ray was estimated as −0.93, corresponding to the vertically linear polarization components of 96.5%. The energy resolution was set to 500 meV, and the base pressure was 1.8×10^{-7} Pa. The samples were cleaved to expose clean (001) surfaces and the measurement temperatures were set to 6 and 10 K for XAS and HAXPES measurements, respectively, both of which were sufficiently lower than the excited states at ∼200 K [31].

The XAS and HAXPES spectra were simulated by making use of full multiplet calculations for Ce^{3+} $3d^{10}4f^1 \rightarrow 3d^9 4f^2$ and $3d^{10}4f^1 \rightarrow 3d^9 4f^1 + e^-$ electric-dipole transitions, respectively, with the XTLS 9.0 program [32]. The atomic parameters of the $4f$-$4f$ and $3d$-$4f$ Coulomb interactions, the $3d$ and $4f$ spin-orbit couplings, were obtained from the Hartree-Fock values for Ce^{3+} [33]. We obtained a reduction factor of 58% (97% and 75%) for the $4f$-$4f$ interaction (spin-orbit couplings for $3d$ and $4f$) by fitting our experimental isotropic Ce $M_{4,5}$ XAS spectrum [15]. The CEF energy for the first (second) excited states $\Delta E_1(\Delta E_2) = 197$ (212) K have been obtained from inelastic neutron scattering (INS) measurements [31].

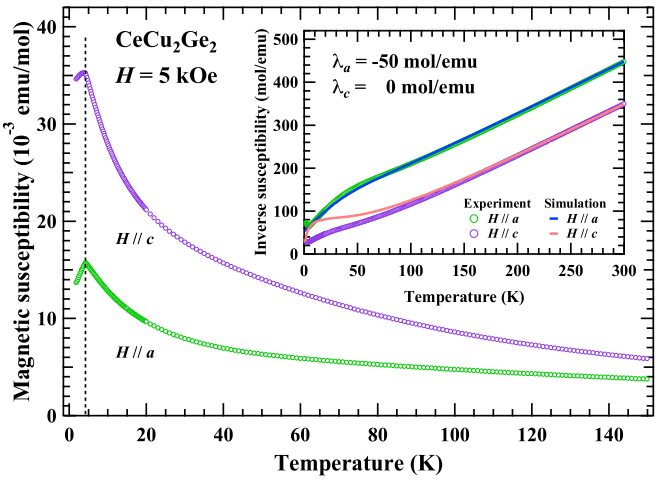

FIG. 3. Anisotropic magnetic susceptibility obtained by applying a magnetic field parallel to the a and c axes. The vertical dashed line indicates T_N. The inset shows the inverse magnetic susceptibility with those obtained by simulation based on the CEF model (solid lines). An anisotropic molecular field parameter of λ_a (λ_c) = −50 (0) mol/emu is taken into account in the simulation along the a (c) axis.

Figure 2 shows the circularly polarized Ce $M_{4,5}$ XAS data of $CeCu_2Ge_2$ (top) measured for photon incidence angles of $\theta = 0°$ and 54.7° relative to the c axis (surface normal). The $\theta = 0°$ geometry yields the XAS intensity with the linear polarization $\vec{E}$ perpendicular to the tetragonal c axis, labeled as $\mu_{\perp c}$, since the electric field vector $\vec{E}$ must be transverse to the direction of light propagation [34]. The spectrum for $\theta = 54.7°$ provides the polarization-averaged isotropic XAS spectrum $\mu_{\rm iso} = (2\mu_{\perp c} + \mu_{\parallel c})/3$, where $\mu_{\parallel c}$ denotes the XAS intensity with $\vec{E}$ parallel to the c axis. The initial-state $4f^0$ components at around 888 eV are negligibly small, indicating a highly localized character of the $4f$ states [18,34]. The $\mu_{\perp c}$ signals deviate from the isotropic spectrum, as shown in the difference spectrum defined as $\mu_{\perp c} - \mu_{\rm iso}$ (bottom), reflecting the orbital anisotropy of the Ce $4f$ states. The spectral simulation rules out the $|\Gamma_7\rangle = \alpha\,|\pm\frac{5}{2}\rangle \pm \sqrt{1-\alpha^2}\,|\mp\frac{3}{2}\rangle$ ground states with $\alpha^2 = 0.81$, since the polarization dependence of the simulated spectra at $M_{4,5}$ edges is too large to account for the experimental data. By fitting the $\mu_{\perp c} - \mu_{\rm iso}$ spectrum (bottom), we find the best-fit parameter of $\alpha^2 = 0.45 \pm 0.05$ for the Γ_7 states, yielding a magnetic moment along the a axis (M_a) of $0.95\mu_B$/Ce as obtained from Fig. 1(a). This value agrees well with the in-plane Ce moment of $1.04\mu_B$ as reported in INS measurements [9,21,23]. Note that a spectral simulation for Γ_6 ground states results in the relative intensity of two multiplet peaks at the M_5 edge different from the experimental signals and thus the possibility of the Γ_6 ground states is excluded.

Figure 3 displays the magnetic susceptibility obtained under an external magnetic field of $H = 5$ kOe parallel to the a and c axes. In the antiferromagnetically ordered phase below T_N, the c-axis susceptibility χ_c is nearly constant, while the a-axis susceptibility χ_a tends to decrease with temperature. This is consistent with the ordered magnetic moment aligned in the ab plane as reported in neutron measurements [23], although

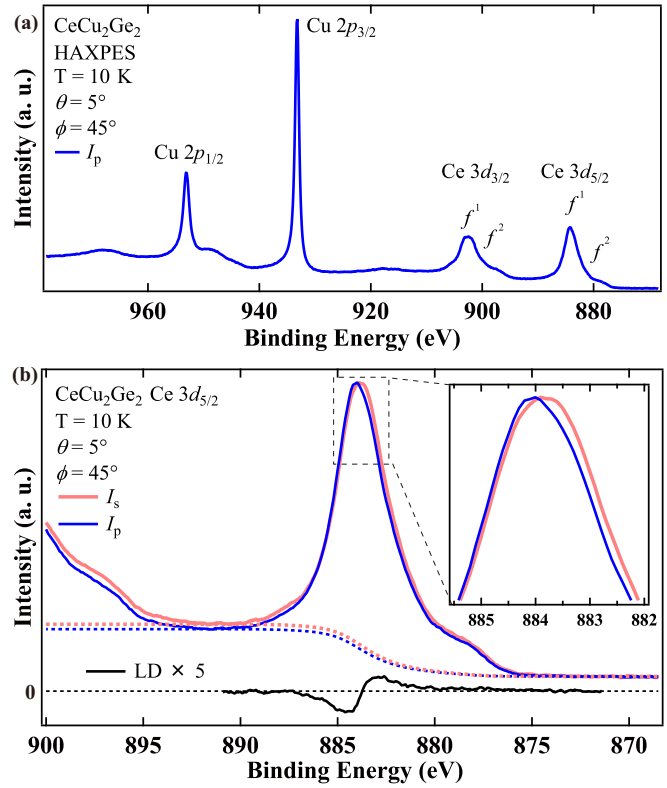

FIG. 4. (a) Ce $3d$ core-level spectrum together with Cu $2p$ states. (b) Polarized Ce $3d_{5/2}$ HAXPES (solid lines) with the backgrounds (dashed line) obtained by the experimental geometry as shown in Fig. 1(b). The thin and thick solid lines denote the photoelectron intensities of I_s and I_p, and corresponding LD is plotted in the bottom. The inset shows an enlarged view around the main $3d_{5/2}$ peak.

χ_a is smaller than χ_c. As shown in the inset, χ_c^{-1} is well reproduced by the simulation of $\chi_{\rm CEF}^{-1}$ given by a standard CEF calculation assuming the Γ_7 ground states with $\alpha^2 = 0.45$ as determined by XAS and the CEF energy of $\Delta E_1(\Delta E_2) = 197$ (212) K [31]. On the other hand, χ_a^{-1} is fitted by using $\chi^{-1} = \chi_{\rm CEF}^{-1} - \lambda_a$, where λ_a is the anisotropic molecular field parameter along the a axis of −50 mol/emu. This suggests that anisotropy of the magnetic exchange interactions between the Ce ions is important for the antiferromagnetic structure.

To determine the rotational symmetry of the Γ_7 ground state, we have performed the Ce $3d$ core-level HAXPES measurements. Figure 4(a) shows an overview of the Ce $3d$ and Cu $2p$ core-level spectra. The Ce $3d$ spectrum shows atomiclike multiplets mainly due to the $3d^9 4f^1$ and $3d^9 4f^2$ final states [35]. The Cu $2p$ spectrum shows sharp peaks without satellite $2p^5 3d^9$ final-state multiplet structures [36,37], indicating that the Cu $3d$ states are fully occupied. Thus the Cu $3d$ states hardly hybridize with the Ce $4f$ states. Figure 4(b) shows the Ce $3d_{5/2}$ spectra obtained by using linearly polarized x rays. As shown in the inset, the intensity obtained with s- and p-polarized configurations labeled as I_s and I_p is switched around the peak top at ∼884 eV. This is highlighted in the linear dichroism (LD) spectrum defined here by the difference of intensity normalized from 871.4 to

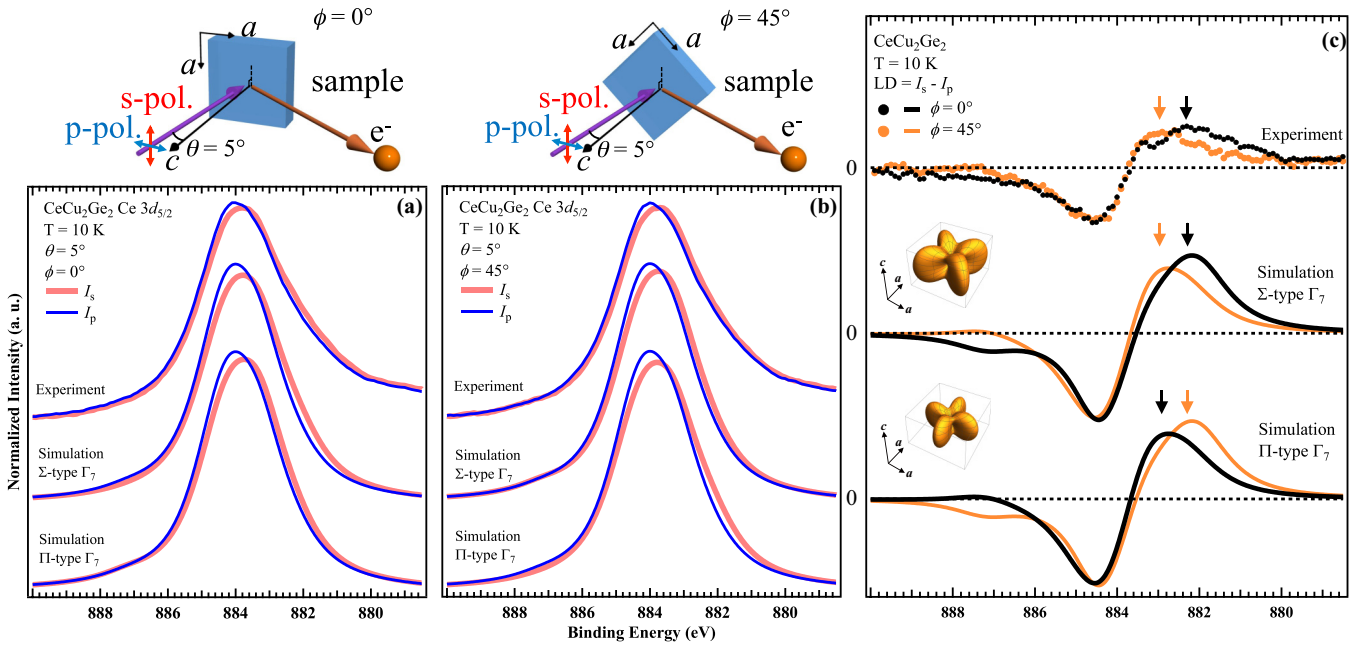

FIG. 5. (a), (b) Linearly polarized Ce $3d_{5/2}$ core-level HAXPES spectra recorded by s- and p-polarized photons together with the spectral simulations assuming the Σ-type Γ_7 and Π-type Γ_7 ground states for the $\phi = 0°$ and 45° configurations. The experimental geometries are illustrated on the top, where the angle between the c axis and the detected photoelectron direction is set to 55°. (c) ϕ-dependent LD obtained by HAXPES and spectral simulations. The error bar of experimental LD spectra is indicated by the size of the markers.

841.6 eV as $I_s - I_p$, after subtracting the background. The sign change of the LD spectrum is attributed to the anisotropic charge distribution of the $4f$ states.

Figures 5(a) and 5(b) show the experimentally observed azimuthal rotation dependence of Ce $3d_{5/2}$ spectra (top) obtained at $\phi = 0°$ and 45°, respectively. Although the difference between I_s and I_p at the higher-energy side of the peak top is similar to each configuration, the dichroism at the low-energy tail around 882 eV in the $\phi = 0°$ configuration is slightly stronger than that in the $\phi = 45°$ spectrum. This tendency is clearly observed in the azimuthal angle dependence of the LD spectra as shown in Fig. 5(c). The major difference between $\phi = 0°$ and 45° configurations is observed in the region with a positive sign of LD spectra between 880 and 883.5 eV, and the positive peak indicated by the arrow of the 45° spectrum is located at the higher-energy side than that of the $\phi = 0°$ spectrum. Azimuthal dependence of the LD spectra is clearly reproduced by the spectral simulation assuming the Σ-type Γ_7 ground states with the same mixing parameter as that obtained by the XAS. Note that Π-type symmetry is obviously ruled out since the spectral simulation shows the opposite trend around 882 eV for the experimental LD spectra. Thus we can identify the in-plane rotational symmetry of Σ-type Γ_7, which is in line with the results of NIXS measurements [19].

The $4f$ symmetry of CEF ground states of the Ce^{3+} ion in $CeCu_2Ge_2$ is thus successfully determined as

$$|\Sigma\text{-type } \Gamma_7\rangle = \sqrt{0.45}\,\left|\pm\tfrac{5}{2}\right\rangle - \sqrt{0.55}\,\left|\mp\tfrac{3}{2}\right\rangle.$$

The in-plane symmetry of $CeCu_2Ge_2$ is the same as that of $CeCu_2Si_2$, which has been reported as $|\Sigma\text{-type } \Gamma_7\rangle = \sqrt{0.77}\,|\pm\tfrac{5}{2}\rangle - \sqrt{0.23}\,|\mp\tfrac{3}{2}\rangle$ [18,38]. Note that the $4f$ charge distribution of $CeCu_2Si_2$ is rather compressed along the c axis in comparison with that of $CeCu_2Ge_2$. Our findings suggest that the c-axis anisotropy of the $4f$ states could play an important role in emerging unconventional superconductivity. Most interesting is that the c-axis anisotropy of $CeCu_2X_2$ (X = Si, Ge) shows a trend opposite to that of $CeIr_{1-x}Rh_xIn_5$ [17], where the $4f$ charge distribution in the superconducting phase expands to the c axis to gain the hybridization with conduction electrons [17]. Therefore, it would be important to take into account the anisotropic hybridization effects, which induce the momentum-dependent heavy electronic structures as reported in the superconductor $CeNi_2Ge_2$ [39]. This motivates us the systematic investigation of $4f$ symmetry for the CeM_2X_2 (M = transition metal) systems to reveal the origin of the quantum criticality.

In conclusion, we have determined the Ce $4f$ symmetry of $CeCu_2Ge_2$ using the combined technique of polarized XAS and core-level HAXPES. The revised out-of-plane anisotropy parameter of α^2 was estimated as 0.45 ± 0.05, which can explain the magnetic properties. The in-plane $4f$ symmetry is Σ type, the same as that of the superconducting $CeCu_2Si_2$, suggesting that the out-of-plane anisotropy plays an essential role in driving the system into the superconducting phase.

We acknowledge S. Takano, K. Nakagawa, M. Murata, and A. Amina for supporting HAXPES measurements. We also thank the support of Y. Takeda of JAEA during the beamtime. The measurements were performed under the approval of BL23SU (Proposals No. 2013B3882, No. 2014B3882, and No. 2016A3832), and BL19LXU (Proposals No. 2014B1305 and No. 2015A1533) at SPring-8. This

work was partly carried out under the Visiting Researcher's Program of the Institute for Solid State Physics, The University of Tokyo. This work was financially supported by Grants-in-Aid for Scientific Research on Innovative Areas (JP20102003, JP16H01074, and JP18H04317), a Grant-in-Aid for Young Scientists (JP23740240), Grant-in-Aid for JSPS Fellows (JP16J00314 and JP16J05334), and a Grant-in-Aid for Scientific Research (JP16H04014, JP18K03537, and JP18K03512) from the Ministry of Education, Culture, Sports, Science and Technology, Japan. Y.N. and K.Y. were supported by the Program for Leading Graduate Schools Interactive Materials Science Cadet Program.

[1] F. Steglich, J. Aarts, C. D. Bredl, W. Lieke, D. Meschede, W. Franz, and H. Schäfer, Phys. Rev. Lett. **43**, 1892 (1979).
[2] H. V. Löhneysen, A. Rosch, M. Vojta, and P. Wölfle, Rev. Mod. Phys. **79**, 1015 (2007).
[3] Q. Si and F. Steglich, Science **329**, 1161 (2010).
[4] O. Stockert, S. Kirchner, F. Steglich, and Q. Si, J. Phys. Soc. Jpn. **81**, 011001 (2012).
[5] Z. F. Weng, M. Smidman, L. Jiao, Xin Lu, and H. Q. Yuan, Rep. Prog. Phys. **79**, 094503 (2016).
[6] K. Hagiwara, Y. Ohtsubo, M. Matsunami, S. Ideta, K. Tanaka, H. Miyazaki, J. E. Rault, P. Le Fèvre, F. Bertran, A. Taleb-Ibrahimi, R. Yukawa, M. Kobayashi, K. Horiba, H. Kumigashira, K. Sumida, T. Okuda, F. Iga, and S. Kimura, Nat. Commun. **7**, 12690 (2016).
[7] O. Trovarelli, M. Weiden, R. Müller-Reisener, M. Gómez-Berisso, P. Gegenwart, M. Deppe, C. Geibel, J. G. Sereni, and F. Steglich, Phys. Rev. B **56**, 678 (1997).
[8] H. Q. Yuan, F. M. Grosche, M. Deppe, G. Sparn, C. Geibel, and F. Steglich, Phys. Rev. Lett. **96**, 047008 (2006).
[9] F. R. de Boer, J. C. P. Klaasse, P. A. Veenhuizen, A. Bohm, C. D. Bredl, U. Gottwick, H. M. Mayer, L. Pawlak, U. Rauschwalbe, H. Spille, and F. Steglich, J. Magn. Magn. Mater. **63–64**, 91 (1987).
[10] Y. Onishi and K. Miyake, J. Phys. Soc. Jpn. **69**, 3955 (2000).
[11] A. T. Holmes, D. Jaccard, and K. Miyake, J. Phys. Soc. Jpn. **76**, 051002 (2007).
[12] K. Miyake and S. Watanabe, Philos. Mag. B **97**, 3495 (2017).
[13] M. Smidman, D. T. Adroja, A. D. Hillier, L. C. Chapon, J. W. Taylor, V. K. Anand, R. P. Singh, M. R. Lees, E. A. Goremychkin, M. M. Koza, V. V. Krishnamurthy, D. M. Paul, and G. Balakrishnan, Phys. Rev. B **88**, 134416 (2013).
[14] The magnetic moment is estimated as $\langle M_a\rangle = \langle\psi^{\mp}|\frac{g_J}{2}(J^+ + J^-)|\psi^{\pm}\rangle$, and $\langle M_c\rangle = \langle\psi^{\pm}|g_J J_z|\psi^{\pm}\rangle$ along the a and c axes [13], where g_J denotes a g-factor of 6/7 for a Ce ion and the quantization axis is set to the c axis.
[15] P. Hansmann, A. Severing, Z. Hu, M. W. Haverkort, C. F. Chang, S. Klein, A. Tanaka, H. H. Hsieh, H.-J. Lin, C. T. Chen, B. Fåk, P. Lejay, and L. H. Tjeng, Phys. Rev. Lett. **100**, 066405 (2008).
[16] T. Willers, D. T. Adroja, B. D. Rainford, Z. Hu, N. Hollmann, P. O. Körner, Y.-Y. Chin, D. Schmitz, H. H. Hsieh, H.-J. Lin, C. T. Chen, E. D. Bauer, J. L. Sarrao, K. J. McClellan, D. Byler, C. Geibel, F. Steglich, H. Aoki, P. Lejay, A. Tanaka, L. H. Tjeng, and A. Severing, Phys. Rev. B **85**, 035117 (2012).
[17] T. Willers, F. Strigari, Z. Hu, V. Sessi, N. B. Brookes, E. D. Bauer, J. L. Sarrao, J. D. Thompson, A. Tanaka, S. Wirth, L. H. Tjeng, and A. Severing, Proc. Natl. Acad. Sci. USA **112**, 2384 (2015).
[18] T. Willers, F. Strigari, N. Hiraoka, Y. Q. Cai, M. W. Haverkort, K.-D. Tsuei, Y. F. Liao, S. Seiro, C. Geibel, F. Steglich, L. H. Tjeng, and A. Severing, Phys. Rev. Lett. **109**, 046401 (2012).
[19] J.-P. Rueff, J. M. Ablett, F. Strigari, M. Deppe, M. W. Haverkort, L. H. Tjeng, and A. Severing, Phys. Rev. B **91**, 201108(R) (2015).
[20] G. Knopp, A. Loidl, K. Knorr, L. Pawlak, M. Duczmal, R. Caspary, U. Gottwick, H. Spille, F. Steglich, and A. P. Murani, Z. Phys. B **77**, 95 (1989).
[21] G. Knebel, C. Eggert, D. Engelmann, R. Viana, A. Krimmel, M. Dressel, and A. Loidl, Phys. Rev. B **53**, 11586 (1996).
[22] A. Krimmel, A. Loidl, H. Schober, and P. C. Canfield, Phys. Rev. B **55**, 6416 (1997).
[23] D. K. Singh, A. Thamizhavel, J. W. Lynn, S. Dhar, J. Rodriguez-Rivera, and T. Herman, Sci. Rep. **1**, 117 (2011).
[24] T. Mori, S. Kitayama, Y. Kanai, S. Naimen, H. Fujiwara, A. Higashiya, K. Tamasaku, A. Tanaka, K. Terashima, S. Imada, A. Yasui, Y. Saitoh, K. Yamagami, K. Yano, T. Matsumoto, T. Kiss, M. Yabashi, T. Ishikawa, S. Suga, Y. Ōnuki, T. Ebihara, and A. Sekiyama, J. Phys. Soc. Jpn. **83**, 123702 (2014).
[25] Y. Kanai, T. Mori, S. Naimen, K. Yamagami, H. Fujiwara, A. Higashiya, T. Kadono, S. Imada, T. Kiss, A. Tanaka, K. Tamasaku, M. Yabashi, T. Ishikawa, F. Iga, and A. Sekiyama, J. Phys. Soc. Jpn. **84**, 073705 (2015).
[26] S. Hamamoto, S. Fujioka, Y. Kanai, K. Yamagami, Y. Nakatani, K. Nakagawa, H. Fujiwara, T. Kiss, A. Higashiya, A. Yamasaki, T. Kadono, S. Imada, A. Tanaka, K. Tamasaku, M. Yabashi, T. Ishikawa, K. T. Matsumoto, T. Onimaru, T. Takabatake, and A. Sekiyama, J. Phys. Soc. Jpn. **86**, 123703 (2017).
[27] B. Zeng, Q. R. Zhang, D. Rhodes, Y. Shimura, D. Watanabe, R. E. Baumbach, P. Schlottmann, and T. Ebihara, and L. Balicas Phys. Rev. B **90**, 155101 (2014).
[28] Y. Saitoh, Y. Fukuda, Y. Takeda, H. Yamagami, S. Takahashi, Y. Asano, T. Hara, K. Shirasawa, M. Takeuchi, T. Tanaka, and H. Kitamura, J. Synchrotron Radiat. **19**, 388 (2012).
[29] M. Yabashi, K. Tamasaku, and T. Ishikawa, Phys. Rev. Lett. **87**, 140801 (2001).
[30] H. Fujiwara, S. Naimen, A. Higashiya, Y. Kanai, H. Yomosa, K. Yamagami, T. Kiss, T. Kadono, S. Imada, A. Yamasaki, K. Takase, S. Otsuka, T. Shimizu, S. Shingubara, S. Suga, M. Yabashi, K. Tamasaku, T. Ishikawa, and A. Sekiyama, J. Synchrotron Radiat. **23**, 735 (2016).
[31] M. Loewenhaupt, E. Faulhaber, A. Schneidewind, M. Deppe, and K. Hradil, J. Appl. Phys. **111**, 07E124 (2012).
[32] A. Tanaka and T. Jo, J. Phys. Soc. Jpn. **63**, 2788 (1994).
[33] B. T. Thole, G. van der Laan, J. C. Fuggle, G. A. Sawatzky, R. C. Karnatak, and J.-M. Esteva, Phys. Rev. B **32**, 5107 (1985).
[34] Y. Saitoh, H. Fujiwara, T. Yamaguchi, Y. Nakatani, T. Mori, H. Fuchimoto, T. Kiss, A. Yasui, J. Miyawaki, S. Imada, H.

Yamagami, T. Ebihara, and A. Sekiyama, J. Phys. Soc. Jpn. **85**, 114713 (2016).

[35] M. Yano, A. Sekiyama, H. Fujiwara, Y. Amano, S. Imada, T. Muro, M. Yabashi, K. Tamasaku, A. Higashiya, T. Ishikawa, Y. Ōnuki, and S. Suga, Phys. Rev. B **77**, 035118 (2008).

[36] Z.-X. Shen, J. W. Allen, J. J. Yeh, J.-S. Kang, W. Ellis, W. Spicer, I. Lindau, M. B. Maple, Y. D. Dalichaouch, M. S. Torikachvili, J. Z. Sun, and T. H. Geballe, Phys. Rev. B **36**, 8414 (1987).

[37] J. Ghijsen, L. H. Tjeng, J. van Elp, H. Eskes, J. Westerink, G. A. Sawatzky, and M. T. Czyzyk, Phys. Rev. B **38**, 11322 (1988).

[38] E. A. Goremychkin and R. Osborn, Phys. Rev. B **47**, 14280 (1993).

[39] Y. Nakatani, H. Aratani, H. Fujiwara, T. Mori, A. Tsuruta, S. Tachibana, T. Yamaguchi, T. Kiss, A. Yamasaki, A. Yasui, H. Yamagami, J. Miyawaki, T. Ebihara, Y. Saitoh, and A. Sekiyama, Phys. Rev. B **97**, 115160 (2018).